

Nonreciprocal Response of Electrically Biased Graphene-Coated Fiber

Asma Fallah¹ and Nader Engheta^{1*}

¹ *University of Pennsylvania, Department of Electrical and Systems Engineering,
Philadelphia, Pennsylvania 19104, USA*

(Dated: March 26, 2024)

Here, we theoretically investigate the nonreciprocal response of an electrically biased graphene-coated dielectric fiber. By electrically biasing the graphene coating along the fiber axis, the dynamic conductivity of graphene exhibits a nonsymmetric response with respect to the longitudinal component of guided-mode wave vectors. Consequently, the guided waves propagating in two opposite directions may encounter distinct propagation features. In this work, the electromagnetic properties, such as modal dispersion and some field distributions are presented, and the strength of nonreciprocity is discussed for different parameters of graphene, such as its chemical potential and material loss. Furthermore, the influence of the radius of the fiber on the nonreciprocal response is investigated. We envision that such nonreciprocal optical fibers may find various potential applications in THz, microwave, and optical technologies.

*Electronic address: engheta@seas.upenn.edu

Graphene, a two-dimensional (2D) one-atom-thick material formed by 2D arrays of carbon atoms, exhibits interesting properties in its electronic and photonic interactions, offering exciting potential applications in THz and optics[1–8]. Single-layer graphene has ultrahigh electron mobility with drift velocity that can be as high as $v_f = c/300$ (v_f is Fermi velocity and c is the speed of light in vacuum) [9]. It has been shown that such DC drift electric current, generated by the DC biasing of a graphene sheet, can break the Lorentz reciprocity for the surface waves along the graphene, providing a significant nonreciprocal response[9–17]. The degree of nonreciprocity is influenced by the speed at which the electrons move (v_0) and by their density (n_0). It has been shown that significant nonreciprocity can be achieved by the mere presence of an electron beam comprising a substantial number of electrons moving with a constant velocity [18, 19] in vacuum.

Unbiased graphene-coated deeply sub-wavelength fiber has been investigated in the past, exhibiting interesting features such as wave guidance along fibers with significantly tiny radius[20]. Here, we consider a dielectric fiber with a graphene coating that is electrically biased with a DC voltage along the fiber axis, and we undertake a theoretical investigation to examine the nonreciprocity of various guided modes in the fiber, resulted from the effects of such electrical bias. We study the strength of nonreciprocity for three types of guided modes; transverse magnetic (*TM*), hybrid (*HE*), and surface plasmon polariton (*SPP*) modes, by presenting their modal dispersion. In addition, we have presented a field distribution for *SPP* mode which clearly show nonreciprocal response. Moreover, the effect of the radius of the fiber is also investigated here. Furthermore, we discuss the influence of the material loss of the graphene coating on the nonreciprocal response and present how it affects the real and imaginary parts of the guided-mode wavenumbers. In this work, time variation is assumed to be $e^{i\omega t}$ with ω being the angular frequency. For simplicity, we neglect the intrinsic nonlocal response of the graphene.

To begin, we point out that the non-biased graphene is characterized by surface conductivity (σ_g is scalar) described by Kubo’s formula [21, 22]. It has been demonstrated in [10] that the dynamic conductivity of biased graphene can be written by considering Galilean Doppler shift model, meaning the electrons in the biased graphene moves as a single body with a constant velocity. In the present work, the drift velocity of electrons is assumed to be along the z -axis, which is the axis of the fiber. As a result, electromagnetic waves with wave vectors having z -component (k_z) parallel or antiparallel with respect to the direction

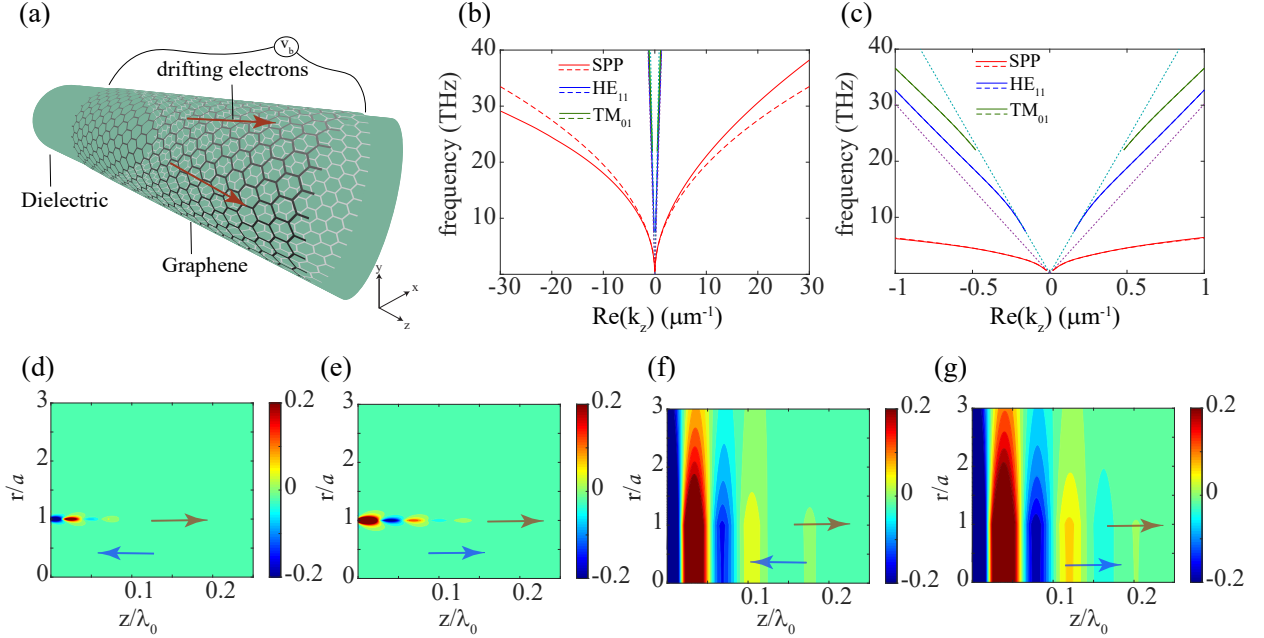


FIG. 1: (a) Schematic of a dielectric fiber coated with a single layer of graphene. V_b denotes the DC bias voltage alongside of the graphene coating. The red arrows conceptually represent the direction of electron drift, depending on the polarity of V_b . (b) Dispersion graphs of the fiber modes, i.e., HE_{11} , TM_{10} , and SPP modes for $v_0 = 0$ and $v_0 = v_f$ shown in dashed and solid lines, respectively. (c) zoomed-in plot around the origin of the panel (b). Dashed cyan and purple lines in (b) and (c) correspond to light lines in the air and fiber. Relative permittivity of the core is $\epsilon_{core} = 2.5$ and its radius is $a = 5 \mu m$. (d-g) Time snapshot of the z -component of the normalized electric field distribution of the guided SPP mode for $f = 15$ THz and radius $a = 5 \mu m$ (d) and (e) and $a = 0.1 \mu m$ (e) and (f). (d) and (f) are for $v_0 = -v_f$ (direction of drift electrons is anti-parallel to the direction of mode propagation). (e) and (g) are for $v_0 = v_f$ (direction of drift electrons is parallel to the direction of mode propagation). Red and blue arrows shows the direction of drift electrons and mode propagation, respectively.

of electron drift velocity in graphene exhibit different interactions with the graphene, since the dynamic surface conductivity adopts two distinct values.

The geometry of the problem of interest is shown in Fig. 1(a), where a dielectric fiber (shown in green) is coated with a single layer of graphene. Here, we employ Maxwell's equations in this guided-wave structure, in analogy with the modal analysis in conventional optical fibers [23]. By incorporating the appropriate boundary conditions and considering the dynamic conductivity of graphene, we analytically derive dispersion relations for various modes: HE_{11} , TM_{10} , and surface plasmon polaritons (SPP), in this graphene-coated optical fiber with a radius of ' a ' and a core relative permittivity of ϵ_{core} . For the HE_{11} mode, denoting $k_0^2 \equiv \omega^2 \mu_0 \epsilon_0$, $k_{r_{core}}^2 \equiv k_0^2 \epsilon_{core} - k_z^2$, and $k_{r_0}^2 \equiv k_z^2 - k_0^2$, the dispersion relation is

given by,

$$\begin{aligned} & \frac{k_z^2 n^2}{a^2 \mu_0 \omega} \left(\frac{1}{k_{r0}^2} + \frac{1}{k_{rcore}^2} \right)^2 XY - \varepsilon_0 \omega \left(\frac{\varepsilon_{core}}{k_{rcore}^2} \frac{Y}{X} + \frac{1}{k_{r0}^2} \frac{X}{Y} + \frac{1 + \varepsilon_{core}}{k_{r0} k_{rcore}} \right) = \\ & \frac{\mu_0 \omega \tilde{\sigma}_\varphi \tilde{\sigma}_z}{k_{r0} k_{rcore}} + i \tilde{\sigma}_z \left(\frac{X}{k_{r0}} + \frac{Y}{k_{rcore}} \right) + i \frac{\tilde{\sigma}_\varphi}{k_{r0} k_{rcore}} \left(\frac{k_z^2 n^2}{a^2} \left(\frac{Y}{k_{r0}^3} + \frac{X}{k_{rcore}^3} \right) - \varepsilon_0 \mu_0 \omega^2 \left(\frac{\varepsilon_{core}}{k_{rcore} X} + \frac{1}{k_{r0} Y} \right) \right) \end{aligned} \quad (1)$$

where $X \equiv J_n(k_{rcore}a)/J'_n(k_{rcore}a)$, $Y \equiv K_n(k_{r0}a)/K'_n(k_{r0}a)$, and n is an integer number, which here is assumed to be 1. In addition, K_n , J_n , μ_0 , and ε_0 are modified Bessel functions of the second kind, Bessel function of the first kind (X' denotes derivation of the function X with respect to its argument), permeability and permittivity in free space, respectively. It is noteworthy that, despite the absence of consideration for nonlocality in this study and the assumption of equal longitudinal (σ_z) and transverse (σ_φ) conductivity in unbiased graphene, the presence of drift electrons yields disparate values for these conductivity components which are $\tilde{\sigma}_z = (\omega/\tilde{\omega}) \sigma_g(\tilde{\omega})$ and $\tilde{\sigma}_\varphi = (\tilde{\omega}/\omega) \sigma_g(\tilde{\omega})$, where $\tilde{\omega} \equiv (\omega - v_0 k_z)$ represents the Doppler-shifted frequency, and $v_0 k_z$ is the inner product of the electron drift velocity with the wave vector of the propagating electromagnetic wave. Furthermore, for the TM_{10} mode with E_z , E_r , and H_φ field components, the dispersion relation is given by,

$$\frac{1}{k_{r0}} \frac{K_1(k_{r0}a)}{K_0(k_{r0}a)} + \frac{\varepsilon_{rcore}}{k_{rcore}} \frac{J_1(k_{rcore}a)}{J_0(k_{rcore}a)} = \frac{i \tilde{\sigma}_z}{\omega \varepsilon_0}. \quad (2)$$

Fig. 1(b) and (c) depict the dispersion characteristics obtained from our analytical expression for biased (solid lines) and unbiased (dashed lines) cases. In this context, we assume a relative permittivity of $\varepsilon_{core} = 2.5$ for the lossless fiber, similar to polymers like Polystyrene [24]. Throughout this study, unless otherwise specified, the chemical potential, scattering rate, and temperature of graphene are assumed to be $\mu_c = 0.4$ eV, $\Gamma = 1/(0.4ps)$, and $T = 300$ K, respectively. Red curves in Fig. 1(b) and (c) present the dispersion diagram of the SPP mode in the fiber, which exhibits a pronounced nonreciprocal response (i.e., wavenumbers of these SPP modes propagating in $+z$ and $-z$ directions are notably non-symmetric). In panel (c) of Fig. 1, which is a magnified view of panel (b) near the origin, dispersion graphs of other guided modes such as HE_{11} and TM_{10} are also depicted. It is

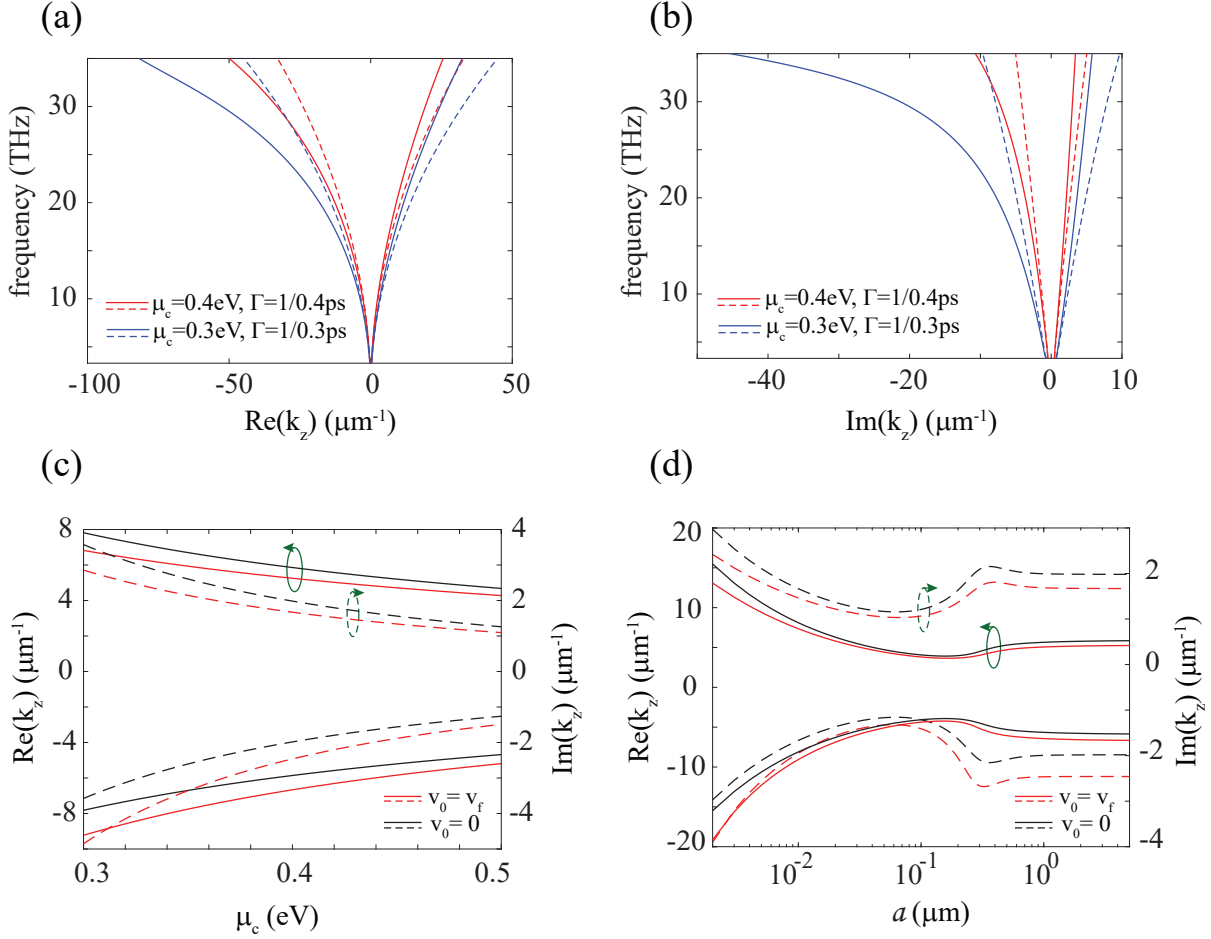


FIG. 2: (a) Real and (b) imaginary parts of wavenumber for biased graphene coating with various scattering rates, here we assume $k_z = Re(k_z) - iIm(k_z)$. Solid and dashed lines represent the biased ($v_0 = v_f$) and unbiased ($v_0 = 0$) cases, respectively. Real and imaginary part of wavenumber of the *SPP* mode at $f = 15$ THz versus (c) chemical potential and (d) the radius of the fiber for $v_0 = v_f$ and $v_0 = 0$.

worth noting that the strength of nonreciprocity manifested in the term ($\tilde{\omega} = \omega - v_0 k_z$) depends upon the relative values of ω and $v_0 k_z$, which implies that in order to achieve a high level of nonreciprocity, these two values should be close to each other. As an illustration, consider the HE_{11} mode at 12 THz, in this case, the disparity between the real parts of the wave vectors of the two propagation directions is quantified by $\Delta k_z = k_z^- + k_z^+ = -30.1442 \times 10^{-6} \mu m^{-1}$ (k_z^+ for (right-going/ $+z$) and k_z^- for (left-going/ $-z$)). Similarly, for the TM_{10} mode at 25 THz, the difference in k_z is $\Delta k_z = -19.1925 \times 10^{-6} \mu m^{-1}$. These differences are much smaller than the values of k_z in HE_{11} and TM_{10} modes. However, the difference in wave vectors for two propagation directions for the *SPP* case is comparatively much larger. This explains why the *SPP* mode demonstrates a robust nonreciprocal response, attributed to

its higher value of k_z and strong field confinement near the graphene coating, in contrast to other modes, which remain practically unaffected.

We also present the field distribution of the *SPP* guided mode at $f = 15 \text{ THz}$ for two distinct polarities of the DC electrical biasing with respect to the guided wave propagation along the fiber for two different radius of fiber in figure 1. Figure 1(d)-(g) present time snapshots of the real part of z -component of normalized electric field profile at $f = 15 \text{ THz}$. In Fig. 1 (d) and Fig. 1(e), radius of the fiber is assumed to be $a = 5 \mu\text{m}$ and the field distributions are plotted for positive ($v_0 = v_f$) and negative ($v_0 = -v_f$) bias polarities, respectively. Similar figures have been demonstrated for $a = 0.1 \mu\text{m}$ case in Fig. 1(f) and Fig. 1(g). These field distributions vividly demonstrate how the *SPP* mode, concentrated around the graphene coating, has been "dragged" or "opposed" by the drift electrons.

In order to elucidate further the nonreciprocal response, we also investigate the influence of graphene loss on the real and imaginary parts of the guided wavenumber for the *SPP* mode. Figures 2 (a) and (b) show the dispersion characteristics of the structure while considering two different values for the electron scattering rate. As demonstrated in Fig. 2(a), the real part of the wavenumber tilts to the left when the graphene is biased, implying that by biasing the graphene coating, the guided *SPP* propagating in the same direction as the drift electrons (right-going/ $+z$), propagates with smaller wavenumber than the opposite direction (left-going/ $-z$). Fig. 2(b) depicts imaginary parts of the wavenumber. This visualization highlights two key aspects: (1) in the presence of a nonzero electrical bias, the left-going/ $-z$ mode experiences stronger attenuation than the right-going/ $+z$ mode. This is due to the plasmons being dragged by the drift electrons in one direction and opposed in the opposite direction; (2) compared with the unbiased case, loss of the wave decreases in the same direction as the drift of electrons while increasing in the opposite direction.

Since the conductivity of graphene can be dynamically tuned using its chemical potential (via chemical doping or electric bias doping), here we explore the role of chemical potential in nonreciprocity of the *SPP* mode. Figure 2(c) shows real and imaginary parts of the *SPP*'s wavenumber at $f = 15 \text{ THz}$ in the presence and absence of the electrical bias as a function of the chemical potential of the graphene coating. The results clearly demonstrate that tuning μ_c allows us to tailor the nonreciprocal response. Hence, based on these findings, it can be inferred that the proposed structure holds potentials for serving as a tunable mid-IR nonreciprocal device.

In this work, we have studied the nonreciprocal response of an electrically biased graphene-coated fiber considering transverse magnetic, hybrid, and surface plasmon polariton modes. We have also presented the effects of the fiber radius, the chemical potential and material loss of graphene coating on the nonreciprocal response and how they are manifested in real and imaginary parts of modal wavenumber. The proposed structure may find possibilities in controlling and manipulating the excited *SPP* modes inside of the graphene-coated optical fibers with potential applications in THz systems, microwave devices, and nanophotonics networks.

The authors express their thanks to Prof. Mário G. Silveirinha of the University of Lisbon for valuable discussions.

This work is supported in part by the National Science Foundation (NSF) Emerging Frontiers in Research and Innovations (EFRI) Program grant #1741693.

-
- [1] A. Vakil and N. Engheta, *Science* **332**, 1291 (2011).
 - [2] V. W. Brar, M. C. Sherrott, M. S. Jang, S. Kim, L. Kim, M. Choi, L. A. Sweatlock, and H. A. Atwater, *Nature communications* **6**, 1 (2015).
 - [3] S. Thongrattanasiri, F. H. Koppens, and F. J. G. De Abajo, *Physical review letters* **108**, 047401 (2012).
 - [4] M. Esquius-Morote, J. S. Gómez-Dí, J. Perruisseau-Carrier, et al., *IEEE Transactions on Terahertz Science and Technology* **4**, 116 (2014).
 - [5] J. Wu, L. Jia, Y. Zhang, Y. Qu, B. Jia, and D. J. Moss, *Advanced Materials* **33**, 2006415 (2021).
 - [6] H. Wang, H. Takamatsu, and X. Zhang, *Handbook of Graphene, Volume 5: Energy, Healthcare, and Environmental Applications* p. 435 (2019).
 - [7] M. Liu, X. Yin, E. Ulin-Avila, B. Geng, T. Zentgraf, L. Ju, F. Wang, and X. Zhang, *Nature* **474**, 64 (2011).
 - [8] M. I. Shaukat and M. G. Silveirinha, in *Metamaterials XII* (SPIE, 2020), vol. 11344, pp. 17–22.
 - [9] T. A. Morgado and M. G. Silveirinha, *ACS Photonics* **5**, 4253 (2018).
 - [10] T. A. Morgado and M. G. Silveirinha, *Physical review letters* **119**, 133901 (2017).

- [11] D. S. Borgnia, T. V. Phan, and L. S. Levitov, arXiv preprint arXiv:1512.09044 (2015).
- [12] D. Correas-Serrano, J. S. Gomez-Diaz, A. Alù, and A. Á. Melcón, *IEEE Transactions on Terahertz Science and Technology* **5**, 951 (2015).
- [13] W. Zhao, S. Zhao, H. Li, S. Wang, S. Wang, M. Utama, S. Kahn, Y. Jiang, X. Xiao, S. Yoo, et al., *Nature* **594**, 517 (2021).
- [14] Y. Dong, L. Xiong, I. Phinney, Z. Sun, R. Jing, A. McLeod, S. Zhang, S. Liu, F. Ruta, H. Gao, et al., *Nature* **594**, 513 (2021).
- [15] S. A. Hassani Gangaraj and F. Monticone, *ACS Photonics* **9**, 806 (2022).
- [16] T. A. Morgado and M. G. Silveirinha, *ACS Photonics* **8**, 1129 (2021).
- [17] T. A. Morgado and M. G. Silveirinha, *Nanophotonics* **11**, 4929 (2022).
- [18] A. Fallah, Y. Kiasat, M. G. Silveirinha, and N. Engheta, *Physical Review B* **103**, 214303 (2021).
- [19] A. Fallah, M. Camacho, and N. Engheta, *IEEE Antennas and Wireless Propagation Letters* **21**, 2201 (2022).
- [20] A. R. Davoyan and N. Engheta, *ACS Photonics* **3**, 737 (2016).
- [21] G. W. Hanson, *Journal of Applied Physics* **103**, 064302 (2008).
- [22] V. Gusynin, S. Sharapov, and J. Carbotte, *Journal of Physics: Condensed Matter* **19**, 026222 (2006).
- [23] K. Okamoto, *Fundamentals of optical waveguides* (Elsevier, 2021).
- [24] N. Sultanova, S. Kasarova, and I. Nikolov, *Acta Physica Polonica A* **116**, 585 (2009).
- [25] S. Buddhiraju, Y. Shi, A. Song, C. Wojcik, M. Minkov, I. A. Williamson, A. Dutt, and S. Fan, *Nature communications* **11**, 1 (2020).
- [26] F. Monticone, *Nature Photonics* **14**, 461 (2020).
- [27] B. Lax, K. J. Button, and L. M. Roth, *Journal of Applied Physics* **25**, 1413 (1954).
- [28] L. Fan, J. Wang, L. T. Varghese, H. Shen, B. Niu, Y. Xuan, A. M. Weiner, and M. Qi, *Science* **335**, 447 (2012).
- [29] D. Correas-Serrano, J. Gomez-Diaz, D. Sounas, Y. Hadad, A. Alvarez-Melcon, and A. Alù, *IEEE Antennas and Wireless Propagation Letters* **15**, 1529 (2015).
- [30] A. M. Mahmoud, A. R. Davoyan, and N. Engheta, *Nature communications* **6**, 1 (2015).
- [31] D. L. Sounas and A. Alu, *Nature Photonics* **11**, 774 (2017).